JOURNAL OF PROPULSION AND POWER
Vol. 13, No. 2, March–April 1997

Vortex Shedding in a Large Solid Rocket Motor Without Inhibitors at the Segment Interfaces

K. W. Dotson,* S. Koshigoe,† and K. K. Pace‡
The Aerospace Corporation, El Segundo, California 90245-4691

The internal acoustic response of the Titan IV Solid Rocket Motor Upgrade (SRMU) is analyzed using pressure oscillation time histories measured during four static firing tests. Pressure oscillations for other large solid rocket motors are caused by vortex shedding at annular inhibitors and acoustic feedback resulting from impingement of the vortices on other inhibitors or on the solid rocket motor nozzle. The SRMU does not have inhibitors, but it is shown that acoustic feedback also defines its pressure oscillations. Vortices are shed around the cavity between the center and aft segments and impinge on the nozzle entrance. The frequencies of the pressure oscillations vary about that of the motor fundamental acoustic mode and generally agree with a simple empirical relationship that has been used to model acoustic feedback. The effect of the SRMU pressure oscillations on dynamics and control of the Titan IV system is minor.

I. Introduction

A NEW solid rocket motor design called the Solid Rocket Motor Upgrade (SRMU) will be integrated with the Titan IV system beginning in late 1996. The SRMU has a lower inert weight and higher propellant weight than the current Titan IV solid rocket motor, and therefore, augments system performance. The SRMU has three segments (forward, center, and aft) and is the only large solid rocket motor in production that does not have annular inhibitors at the segment interfaces to prevent combustion and to support the propellant grain during burning.

A. SRMU Static Firing Tests

Five static firing tests were conducted for qualification of the SRMU. The test articles included one preliminary qualification motor (called PQM1′) and four qualification motors (called QM1, QM2, QM3, and QM4). The tests were conducted vertically, nozzle down at the Phillips Laboratory 1-125 Firing Complex, Edwards Air Force Base.[1] The test configuration and the attachments of the solid rocket motor to the test stand simulated flight. The physical differences between the five test motors were minor and are believed to have had a negligible effect on combustion stability. The static firing tests were conducted at propellant bulk temperatures in the range 36.5–93°F (2.5–33.9°C) to assess the effect on motor performance.

The static firing test instrumentation included Condec gauges (CCC-406) of absolute pressure on the forward closure (measurement PCF1) and on the aft dome (measurement PCA1), and a Kistler gauge (202M122) of oscillatory pressure (measurement PD4) on the forward closure.[2] Measurements PCF1 and PCA1 were recorded by a Neff digital acquisition system, while measurement PD4 was recorded by a Metraplex FM system. The Neff system applied a 100-Hz low-pass filter and recorded measurements PCF1 and PCA1 at 250 samples/s. A 100 Hz antialiasing filter was used prior to digitization of measurement PD4 at 1000 samples/s. The data acquisition systems were activated 35 s prior to ignition and continued until 180 s after ignition. The test motors were quenched by a water deluge system that initiated 157 s after ignition.

Although measurements PCF1 and PCA1 had a coarser resolution than measurement PD4 in time (4 vs 1 ms/sample) and in amplitude (0.25 vs 0.02 psi/quantum), reasonable agreement in the frequency content and amplitudes of the pressure oscillations measured by these different transducers was observed. The SRMU results presented herein are based on measurement PD4. However, because this transducer malfunctioned during the QM4 static firing test, a family of four, rather than five, time histories were used to assess test-to-test variability.

B. Effects of Pressure Oscillations on Titan IV System

Two SRMUs are strapped onto the Titan IV core. Lateral support is provided at both the forward and aft attachments of the SRMUs and core. Axial restraint is provided only at the aft end of the vehicle. Axial loads generated by SRMU pressure fluctuations, therefore, are transmitted to the Titan IV core only at its base.

A dynamic analysis was conducted to assess the impact of SRMU thrust oscillations on spacecraft loads.[3] Pressures measured during the static firing tests were used to generate the thrust time history and worst-case phasing of the thrust oscillations for the two SRMUs was assumed. The analysis showed that the oscillatory axial loads transmitted at the aft attachment are damped by the core and that the spacecraft loads induced by the thrust oscillations are enveloped by those for other loads events. Not all launch vehicles connect solid rocket motors to the core like the Titan IV system. The Space Shuttle and the Ariane 5 launch vehicles, for example, provide axial restraint at the forward attachment. Thrust oscillations for these vehicles have a greater potential for generating significant spacecraft loads. The thrust oscillations are also not a concern for the Titan IV launch vehicle itself because prelaunch conditions, liftoff, and the maximum acceleration event define its axial load environment. Finally, rigid body responses induced by the thrust oscillations are very small, and the frequencies of the thrust oscillation are much higher than the bandwidth of the vehicle autopilot.

Although the impact of the SRMU pressure oscillations on dynamics and control of the Titan IV system was determined to be minor, a study was conducted to better understand the source of the oscillations. The effect of pressure oscillations on the

Received July 25, 1995; revision received April 18, 1996; accepted for publication July 19, 1996.

*Engineering Specialist, Structural Dynamics Department, 2350 East El Segundo Boulevard. Member AIAA.

†Senior Member of Technical Staff, Fluid Mechanics Department, 2350 East El Segundo Boulevard. Senior Member AIAA.

‡Senior Member of Technical Staff, Propulsion Department, 2350 East El Segundo Boulevard. Member AIAA.

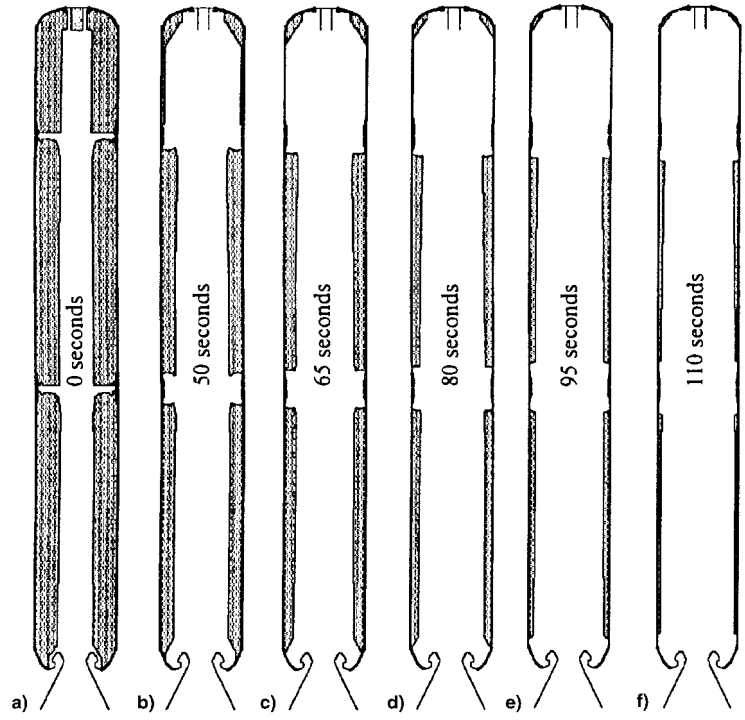

Fig. 1 SRMU internal geometry during burn.

combustion stability of solid rocket motors has received considerable attention because of its potentially catastrophic impact on flight systems.[4] The presentation of results for a large solid rocket motor without inhibitors at the propellant segment interfaces provides an opportunity to enhance the state of knowledge in this field. This study involves a comprehensive analysis of the SRMU static firing test data and examination of the available literature. Simple empirical models and linear theory, which are amenable to industrial applications, are emphasized.

II. SRMU Test Data

The SRMU propellant surface is shown in Fig. 1 for several burn times. Time $t = 0$ s corresponds to ignition. Note that, as the propellant burns, the cavities at the segment interfaces become wider and shallower.

A. Time Domain Results

Representative pressure time histories for a static firing test (QM3) are provided in Fig. 2. The absolute pressure (measurement PCF1) in the forward closure is shown in Fig. 2a. The pressure oscillations, which are superimposed on the instantaneous mean pressure, are barely discernible in this plot. The time history of oscillatory pressure (measurement PD4) is shown in Fig. 2b. The amplitudes of the pressure oscillations increase at approximately 53 s. A time-expanded window of this signal is shown in Fig. 2c. The beating phenomenon evident in this plot suggests that the pressure oscillations consist of closely spaced frequency components.

The maximum (0-to-peak) amplitude of the pressure oscillations during each of the four static firing tests fell in the range 2.18–2.35 psi (15.0–16.2 kPa) and occurred between 57–63.5 s. The (0-to-peak) amplitudes equaled 0.25–0.27% of the instantaneous absolute pressure. The test-to-test variations in the maximum amplitude and its time of occurrence were therefore small. The dimensions, physical characteristics, and pressure oscillation data for the Titan IV SRMU are compared in Table 1 with published data for other large solid rocket motors.

B. Frequency Domain Results

Spectral density of the pressure oscillations was computed for each of the four static firing tests for which transducer PD4 functioned. The contour waterfall plot of spectral density for the QM3 static firing test is shown in Fig. 3, in which the darkest regions represent the highest spectral density. Color contour waterfall plots for all four of the static firing tests were presented in Ref. 8. The frequencies indicated by the waterfall plots formed the basis for the present study.

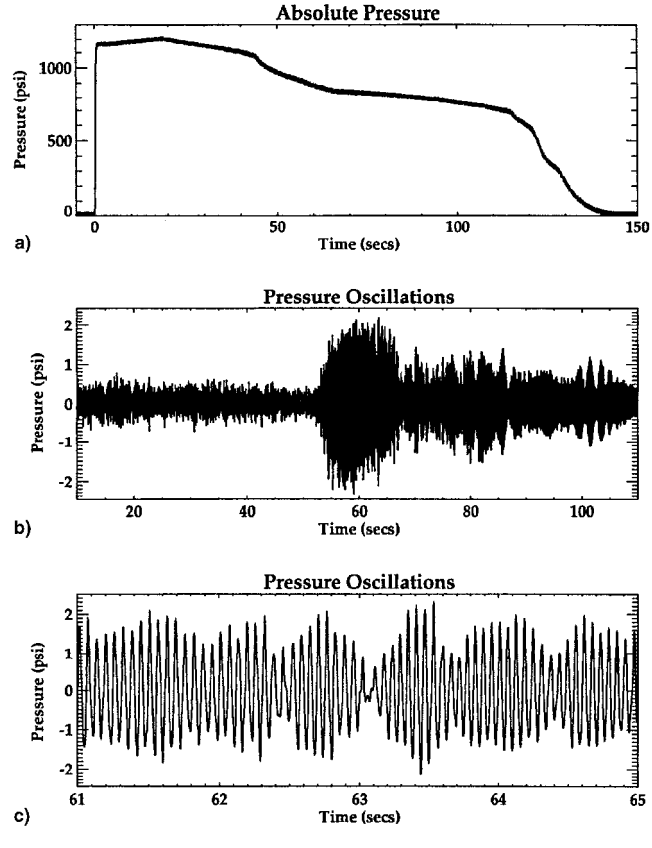

Fig. 2 Representative pressure time histories. QM3 static firing test.

Table 1 Comparison of large solid rocket motors and corresponding published vortex-induced pressure oscillation data

	Physical description[5]					Vortex-induced pressure oscillation data[a]				
Large solid rocket motor	Total length, ft, [m]	Diameter, ft, [m]	Number of segments	Inhibitors at segment interfaces?	Duration of nominal burn, s	Acoustic modes excited	Maximum pressure oscillation (0-to-peak), psi, [kPa]	Maximum pressure oscillation (0-to-peak)/ mean pressure, %	Time of occurrence of maximum pressure oscillations, s	Maximum thrust oscillation/ mean thrust, %
Titan 34D SRM[6,7]	90.4 [27.6]	10.2 [3.1]	5-1/2[b]	Yes	116	1	——	——	——	——
						2	——	——	——	——
Titan IV SRM	112.0 [34.1]	10.2 [3.1]	7[b]	Yes	122	——	——	——	——	——
Titan IV SRMU[8]	112.4 [34.3]	10.5 [3.2]	3	No	138	1	2.4 [16.2]	0.27	57–64	1.5–2
Space Shuttle SRB[9]	149.2 [45.5]	12.4 [3.8]	4	Yes	123	1	——	0.25[c]	70–75	——
						1	——	0.48[c]	110–115	——
						2	——	——	——	——
Ariane 5 MPS[10]	102.0 [31.2]	10.0 [3.0]	3	Yes	123	1	3.7 [25.5]	0.5	90–95	2–4
						2	——	0.2	65–70	——

[a]Values were not reported in the cited references for the fields marked (——).
[b]Not including the forward and aft closures.
[c]Peak-to-peak values are reported in Ref. 9 for ground test and flight motors. The values tabulated here are 0-to-peak for the flight motors, taken as one-half of the published peak-to-peak values.

The spectral analysis was conducted using the maximum entropy method (MEM), one of several spectral analysis techniques suitable for nonstationary data. In this approach, the order and the coefficients of a finite autoregressive prediction filter are estimated, and the spectral estimate has a form similar to the frequency response function of an all pole digital filter.[11] A mathematical development of the maximum entropy method is provided in Ref. 12.

MEM is particularly suited to rapidly varying signals because short time segments can be used without affecting the frequency resolution of the spectrum. If care is taken in the selection of the number of poles, sharp spectral peaks can be defined, an advantage in the assessment of vortex shedding.[13] The maximum entropy method was also used in Ref. 14 for the analysis of solid rocket motor responses driven by combustion.

Five hundred poles were used for the MEM analysis of the SRMU pressure oscillations. The corresponding spectral peaks match the frequencies of, but are much sharper than, those for fast Fourier transform- (FFT-) based spectral density. Splitting of spectral peaks, which can result if an excessive number of poles is used in the maximum entropy method, did not occur. The Wigner–Ville distribution[11] and interpolation of FFT-based spectral density via zero padding[12] were also explored, but were found to be less effective than MEM for the visualization of the pressure oscillation frequencies. Kalman filtering could not be implemented because the current algorithms require a tracking signal[11] and it is unclear how this signal could be defined for the pressure oscillation data.

Spectra were computed over 2-s time windows with a 1-s overlap between adjacent spectra. The pressure oscillations for $t < 50$ s and $t > 110$ s are small with respect to those for $t = 50–110$ s, and the frequency content for these time periods can be ignored. Similarly, components of the pressure oscillations outside of the frequency range 14–20 Hz are negligible.

As shown in Fig. 3, the components of the pressure oscillations are grouped in tracks, in which frequency decreases with time. It is also evident that the pressure oscillations are often represented by a single frequency, but can consist of two components for a few seconds and, even more briefly, of three. The closely spaced frequency components cause the time history of the pressure oscillation to beat, as shown in Fig. 2c. The difference between the frequencies is approximately equal to the inverse of the time between the beats. For example, Fig. 2c has beat maxima at about $t = 62.75$ and 63.45 s. The two frequencies of the MEM spectrum at $t = 62$ s (defined by the time window 62–64 s) should, therefore, be 1/0.7 = 1.4 Hz apart. The QM3 waterfall plot (see Fig. 3) corroborates this result. Checks of the accuracy of the frequencies indicated by the MEM spectra were conducted by verifying the magnitudes of the frequency jumps corresponding to the signal beating and by manually counting the number of cycles in short time segments at arbitrary time points.

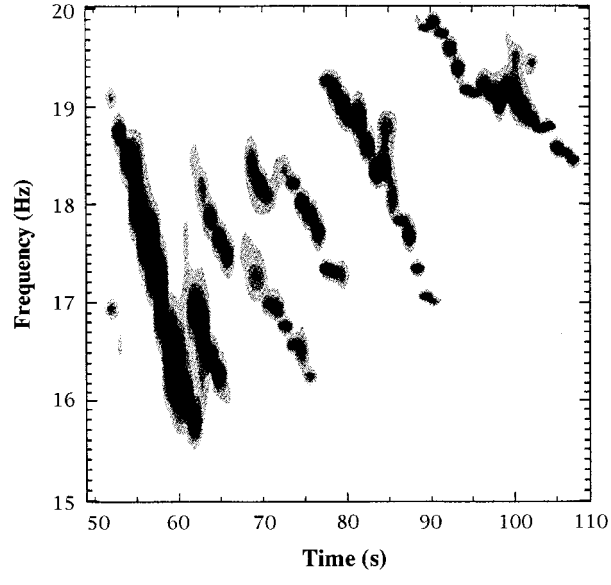

Fig. 3 Contour waterfall plot of spectral density for QM3 static firing test pressure oscillation time history.

Data points that define the frequency tracks of the static firing test waterfall plots were recorded manually using our graphics software and point-and-click cursor selection. Automatic rescaling, introduced upon zooming of time and frequency regions, facilitated the logging of low-amplitude components. The data points were divided into two groups to provide an indication of the amplitudes of the frequency components. Open and closed data points correspond to MEM spectral peaks less than, and greater than, 1 psi^2/Hz (47.5 MPa^2/Hz), respectively. Comparisons of bandpass-filtered time histories with MEM spectra throughout the burn indicate that

spectral peaks greater than 1.0 psi^2/Hz correspond to frequency components with 0-to-peak amplitudes greater than roughly 0.5 psi (3.4 kPa). Because the peaks in the MEM spectra can be sharp or broad, depending on the number of poles, the 1.0-psi^2/Hz threshhold is relevant only for the 500 poles and 2-s time windows used. Scaling in the MEM algorithm, however, ensured that the integral of any given MEM spectrum is identical to that that would be obtained from an FFT-based spectrum using a Hanning window and the same time interval. The MEM spectrum, therefore, has sharp spectral peaks with the same rms value of pressure as the corresponding FFT-based spectrum.

Time profiles for the recorded frequency tracks were next scaled to account for propellant burn rate differences between the static firing tests caused by differences in the propellant bulk temperature and small variations in propellant composition. The scaling factor for a given static firing test was defined as the ratio of the nominal to the test web action times, where the nominal web action time is defined in the SRMU specifications and corresponds to a propellant bulk temperature of 60°F (15.6°C). A database for plotting and manipulation was finally compiled from the scaled results for the four tests.

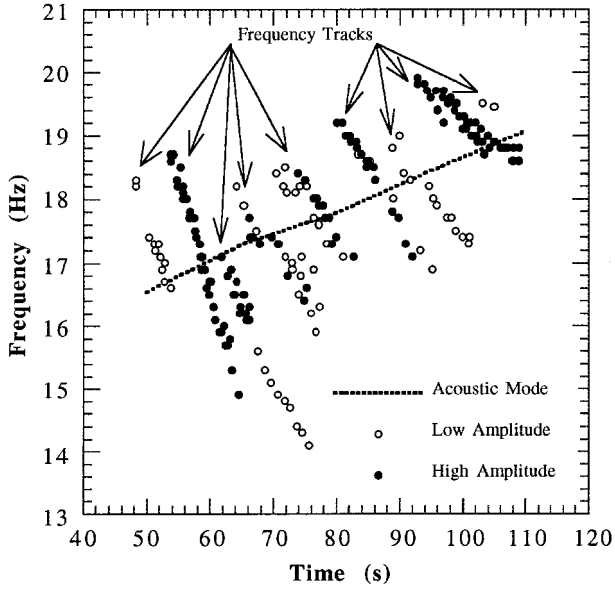

Fig. 4 Comparison of static firing test pressure oscillation frequencies with predicted frequency of fundamental acoustic mode.

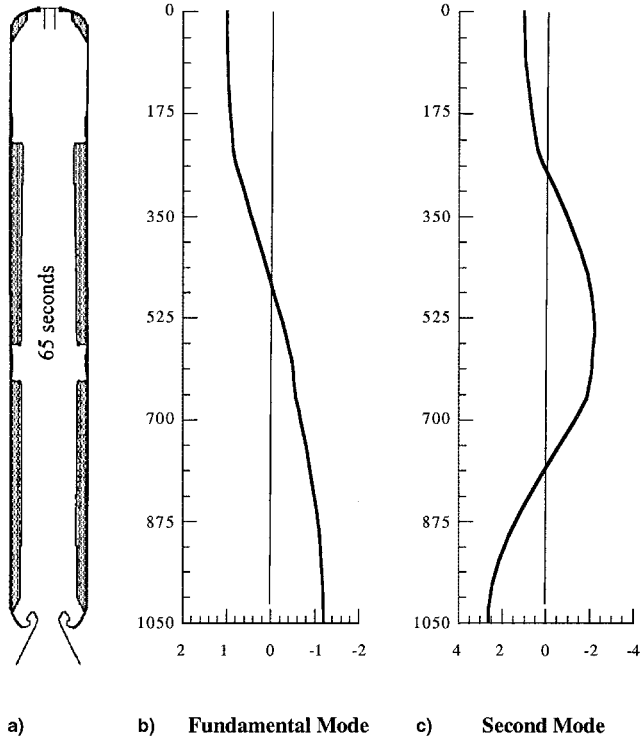

Fig. 5 SRMU internal geometry and mode shapes of acoustic pressure at t = 65 s.

The test results are compared in Fig. 4 with the predicted frequencies of the fundamental acoustic mode. The standard stability prediction module of the solid propellant rocket motor performance (SPP) computer code[15] was used to compute the frequencies of the acoustic modes and the mode shapes shown in Figs. 5b and 5c.

Nine frequency tracks are evident in Fig. 4, if the two open data points at t = 103 and 105 s are grouped. None of the four static firing tests are individually sufficient to define all of the frequency tracks exhibited by the compiled results.

The frequency tracks intersect the frequency of the fundamental acoustic mode. The pressure oscillation amplitudes are largest at time points when the frequencies of the acoustic mode and the pressure oscillations match, a point noted in numerous studies of solid rocket motor data.[6,9,10,16] The maximum pressure oscillations occur around the intersection defined by t = 59 s.

III. Vortex Shedding in Solid Rocket Motors

A. Brief Historical Summary

The periodic shedding of vortices caused by obstructions was first suggested by Flandro and Jacobs[17] as a potential source of acoustic energy in ducts and chambers. Brown et al.,[6] Flatau and VanMoorhem,[16] and Scippa et al.[10] documented studies of pressure oscillations measured during static firing tests of the Titan 34D, Space Shuttle, and Ariane 5 solid rocket motors, respectively. In all three of these publications, subscale cold-flow simulations were used to corroborate the finding that the observed pressure oscillations were produced by coupling between the solid rocket motor acoustic modes and vortex shedding from inhibitors protruding into the internal flow. Experiments conducted by Culick and Magiawala,[18] Dunlap and Brown,[19] and Nomoto and Culick[20] of flow over baffles in a chamber demonstrated coupling of the frequencies of the periodic vortex shedding with those of the acoustic modes of the chamber. A linear theory was derived by Flandro,[21] which models the vortex shedding phenomenon and is intended for practical system analysis. Computational fluid dynamics (CFD) has also been used recently by Vuillot et al.[22,23] and Kourta[24] for numerical simulation of the unsteady internal flow in solid rocket motors.

In this work a simple empirical relationship is used to provide a plausible physical explanation for the pressure oscillations measured during the Titan IV SRMU static firing tests. Variations of this approach were used by Flatau and VanMoorhem[16] and Nesman[9] in their analysis of Space Shuttle solid rocket booster (SRB) pressure oscillations and have also been used to explain vortex shedding observed in a wide variety of shear layer and impingement edge configurations.[20,25]

B. Acoustic Feedback Model

In this section the acoustic feedback model is described and the empirical relationship is derived. In Sec. IV, sensible assumptions about the SRMU internal flow are made to establish the model parameters; the published linear theory, experimental results, and CFD analyses are used to substantiate these claims. The predicted frequency variations are finally compared in Sec. V with those identified from the static firing test data.

The fundamental steps of the acoustic feedback model are as follows:

1) A shear layer is generated at an upstream point and rolls up into a vortex as it travels downstream.

2) The vortex impinges on a surface.

3) An acoustic pulse is generated by the vortex impingement and travels back upstream.

4) The acoustic pulse reaches the shear-layer initiation point and perturbs the shear layer at the right time to contribute to a subsequent vortex.

5) A new vortex rolls up, closing the feedback loop.

It is implied in the previous description that an integer number of vortices fit between the shear-layer initiation and impingement points. This is supported by the visualization of vortices between baffles in a duct conducted by Nomoto and Culick.[20]

The feedback loop can be expressed mathematically as[25]

$$mT = L/kU + L/(c - U) + \Delta t \tag{1}$$

in which T is the period of the vortex shedding, L is the distance between the shear-layer initiation and impingement points, U is the freestream velocity, c is the speed of sound, m is the number of vortices lying between the shear-layer initiation and impingement points, k is the ratio of the velocity at which the vortices are convected to the freestream velocity, and Δt is a small time increment. The value k is a dimensionless empirical constant. The value m is called the stage number.

The first and second terms on the right-hand side (RHS) of Eq. (1) represent, respectively, the time that elapses between steps 1 and 2, and steps 3 and 4 of the acoustic feedback model; the third term, Δt, accounts for the delay between the impingement of a vortex and the generation of an acoustic pulse, that is, the time that elapses between steps 2 and 3. This correction factor is commonly expressed as αT, in which α is a dimensionless empirical constant.

Solving Eq. (1) for the vortex shedding frequency f yields

$$f = \frac{U}{L}\left\{\frac{m - \alpha}{[M/(1 - M)] + 1/k}\right\} \tag{2}$$

in which M is the Mach number. Expanding the first term in the denominator of Eq. (2) into a binomial series and truncating after the first term yields

$$f = \frac{U}{L}\left(\frac{m - \alpha}{M + 1/k}\right) + \mathcal{O}(M^2) \tag{3}$$

The Strouhal number Sr for the feedback loop is finally defined by

$$Sr = \frac{fL}{U} = \frac{m - \alpha}{M + 1/k} \tag{4}$$

The Mach number for the internal flow of large solid rocket motors is small and some investigators have neglected its effect entirely.[16] The predictions of frequency and Strouhal number presented herein, however, were computed using Eqs. (3) and (4). The truncation introduced in Eq. (3) has a negligible effect on the predictions over the range of Mach numbers for the SRMU.

Equation (3) was first proposed by Rossiter[26] for airflow over rectangular cavities. In this case a boundary layer exists and separates at the upstream cavity face, generating vortices that impinge on the downstream cavity face; the stage number m of the acoustic feedback model refers to the number of vortices within the cavity.

C. Implementation of Model for Solid Rocket Motors

The internal flow of solid rocket motors is composed of streamlines generated at the burning propellant surface that turn and travel parallel to the motor axis. If the motor has multiple segments and inhibitors, a shear layer can initiate at an inhibitor and roll up into vortices that travel downstream and impinge on a downstream inhibitor or on the nozzle.[6] In this case the stage number m of the acoustic feedback model refers to the number of vortices that lie between the upstream inhibitor and the impingement surface. Tests conducted by Vuillot et al.[22,23] of a subscale motor (called LP3-D), with only one segment interface and no inhibitors, demonstrated that propellant surface discontinuities can also generate pressure oscillations. The present work appears to be the first effort to apply the empirical model to this type of motor configuration.

The frequency tracks shown in Fig. 4 are consistent with Eq. (3) and the concept of coupling between the fundamental acoustic mode and vortex shedding; when the frequency of the vortex shedding decreases (because of the reduction in velocity U) to the extent that it is effectively decoupled from the frequency of the acoustic mode, the vortex shedding frequency is increased by the addition of vortices (increase in the integer m) in the distance L.

More sophisticated models that include additional flow parameters exist for the prediction of vortex shedding frequencies. Jou and Menon,[27] for instance, developed a complex-valued characteristic equation whose frequency solutions also depend on two transfer coefficients and the growth rate of the vortical disturbances. These values are not known, and have not been estimated, for the SRMU. However, it can be shown that the frequencies from the Jou and Menon model[27] converge to Eq. (3) (with $\alpha = 0$) for the conditions experienced by the SRMU. [The characteristic equation in Jou and Menon's solution[27] has an exponential dependence on the Mach number and mode number (vortex shedding stage number); it simplifies dramatically for the low Mach numbers typical of large solid rocket motors, and for the stage numbers ($m > 5$) that the SRMU seems to experience. The Jou and Menon solution[27] is intended for ramjets and is weakly dependent on the inlet duct length, dump plane location, and the ratio of the inlet duct and dump plane diameters. Equation (3) results if 1) the inlet duct is taken as the distance from the motor's forward closure to the vortex shedding point, 2) the vortex shedding point acts as the dump plane and lies half of the distance to the nozzle, and 3) the restrictor or propellant grain corner causing the vortex shedding does not protrude very far, relative to the diameter of the motor, from the propellant grain face.]

It is instructive to compare the assumptions for the acoustic feedback model with vortex visualization from CFD analyses. Figures in Ref. 22 show that the length of the vortices is not constant, as suggested by Eq. (1), but increases somewhat with distance from the origin. Also, adjacent vortices may combine to form a single vortex, which has the effect of halving the frequency of the pressure oscillations.[28] CFD analyses conducted by Kourta,[24] however, indicate that the vortex shedding mechanism for high values of dynamic viscosity does not exhibit vortex pairing and is more regular than that for low values of dynamic viscosity. Only the frequency components shown in Fig. 4 were evident in SRMU pressure measurements at both the forward and aft closures. The pairing of vortices, therefore, does not appear to have occurred during the SRMU burn.

IV. SRMU Vortex Shedding Model

A. Definition of Velocity

The values kU and c in Eq. (1) represent, respectively, the average speed of the vortices and sound over L. Variations in the speed of sound are small for the SRMU and, because they affect only the Mach number, have a very minor impact on the vortex shedding frequencies. In this work, the vortex convection speed is defined as a fraction of the freestream velocity at the presumed origin of the vortex shedding. Variations in the speed at which the vortices travel between the shedding and impingement points are assumed to be accounted for in k. Adjustments of k have been employed to account for a deceleration of vortices traveling toward the impingement point.[16,27]

Table 2 Reference values of constants in acoustic feedback empirical model

Reference	Use	k	α	M	m
16	SRM	0.6	0	0.03–0.1	1–4
27	Ramjet	0.5, 0.6	0	0.3, 0.4	1–2
26	Cavity	0.57	0.25	0.4–1.2	1–4
29	Cavity	0.57	0.25	0.2–3.0	1–5

Also note that the freestream velocity is not a constant within solid rocket motors. From the center/aft segment interface of the SRMU to the nozzle it increases at a rate of roughly 2 (in./s)/in. If the speed of the vortices were a function of the freestream velocity throughout the motor, the vortices would accelerate aft of the shedding point. CFD analyses conducted for the Ariane 5 Moteur à Propergol Solide (MPS), however, did not identify frequency differences between the vortex shedding and impingement points, which could be attributed to an axial increase in the mean flow speed.[22]

Empirical values of k and α found in the literature are listed in Table 2. The ranges of m and M over which the values were applied are also shown. Data for a ramjet and cavity tones are included for comparison, although the mean flow is different than that for solid rocket motors. The more complicated expression derived by Jou and Menon[27] required the convection velocity constants listed. For cavity tones, the acoustic pulse propagates within the cavity, in which the mean flow is considered negligible. The second term on the RHS of Eq. (1), therefore, equals L/c for cavity tones and the empirical model can be used for $M > 1$. The empirical values that yielded a best fit for the SRMU static firing test data are $k = 0.58$ and $\alpha = 0.25$.

B. Vortex Shedding Initiation and Impingement Points

As shown in Fig. 1b, the forward segment of the SRMU has essentially burned out by the time the pressure oscillations begin to increase in amplitude. Changes in the internal geometry of the motor that could generate sheared flow, therefore, only exist at the cavity between the center and aft segments. This cavity varies in length and depth with burn time, and, as shown in Fig. 5, lies near a pressure node (velocity antinode) of the fundamental acoustic mode and a pressure antinode (velocity node) of the second acoustic mode. The latter conditions facilitate coupling with the fundamental acoustic mode and suppress coupling with the second acoustic mode.[6]

C. Implementation of Linear Theory

The linear theory developed by Flandro[21] was used to help predict the shear-layer initiation and impingement points. Three scenarios were considered: 1) shear-layer initiation around the forward face of the cavity with impingement on the nozzle entrance, 2) shear-layer initiation around the aft cavity face with impingement on the nozzle entrance, and 3) shear-layer initiation around the forward cavity face with impingement on the aft cavity face.

Some distance may be required before vortices form from initial instability waves and it is unlikely that the vortex shedding initiation point is located exactly at either of the two faces of the cavity. This seems to be confirmed by CFD analyses of cavity-induced vortex shedding in solid rocket motors conducted by Vuillot et al.[23] For the purposes of this study, however, the lengths required for the empirical model will be based on the distance from these faces to the impingement point, with the understanding that some uncertainty in these values probably exists.

Flandro[21] defines the acoustic growth rate as a product of a scalar and two functions, f (called F in this study to avoid confusion with frequency), and g. The shear-layer origin and impingement points define F, whereas g depends primarily on the shear-layer momentum thickness, the distance between the shear-layer origin and impingement points, and a Strouhal number defined by

$$Sr_m = 2\pi f(\delta/U) \tag{5}$$

in which f is the frequency of the vortex shedding, δ is the shear-layer momentum thickness, and U is the mean flow velocity at the shear-layer origin.

For the three vortex shedding scenarios previously defined, F varies approximately linearly with time. Values of F are provided in Table 3 for time points spanning the period of the significant pressure oscillations. Because F is always negative in Table 3, the function g must also be negative for a positive acoustic growth rate.

Data from CFD analyses conducted by Chang et al.[30] for the redesigned SRMU propellant grain configuration were used to compute the shear-layer momentum thickness at the cavity between the center and aft segments. Velocity profiles were constructed for the flow at $t = 40$ s. Data for other time points were not extant. The normalized profiles for the flow forward of, and in the middle of, the cavity are shown in Fig. 6. Using a planar solution, which is suitable because the radial distance to the cavity is large,[21] the shear-layer momentum thicknesses for these profiles equal $\delta = 4$ in. (10 cm) and 5.5 in. (14 cm), respectively. The zero velocity condition at the propellant surface was not enforced in Ref. 30 because the required boundary elements would have added complexity unnecessary for the assessment of propellant grain deformation, the objective of the CFD analysis. However, the effect of this boundary condition on the integration from the propellant surface to the motor centerline should be very small.

Analytical predictions of U and M (at the center of the cavity) and of L (from the forward cavity face to the nozzle entrance) are listed in Table 4 for several time points. The length L_c and depth D_c of the cavity between the center and aft segments are also provided. The grain design and ballistics mod-

Table 3 Values of growth rate function F in linear theory[21]

Vortex shedding scenario		Values of F	
Origin	Impingement	$t = 50$	$t = 110$
Forward cavity face	Nozzle entrance	−0.08	−0.04
Aft cavity face	Nozzle entrance	−0.17	−0.23
Forward cavity face	Aft cavity face	−0.17	−0.12

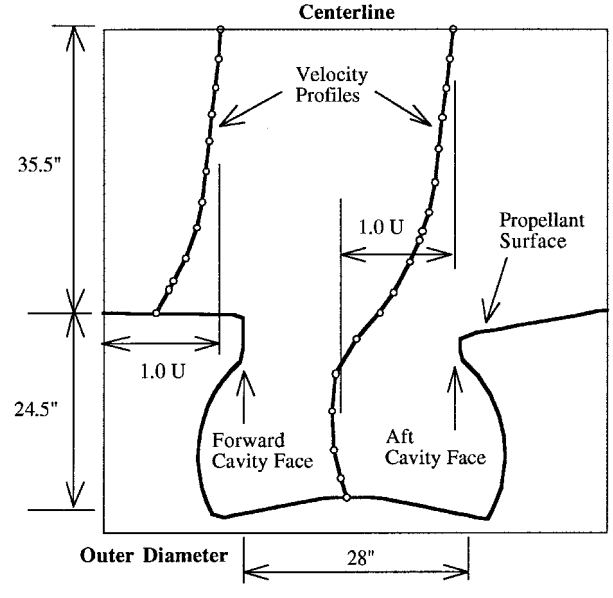

Fig. 6 Deformed propellant grain and velocity profiles at the center/aft segment interface for $t = 40$ s.

Table 4 Analytical predictions of SRMU internal flow, grain geometry, and Strouhal number Sr_m at the cavity between the center and aft segments

t, s	U, in./s, [m/s]	Sr_m	L, in., [m]	M	L_c, in., [cm]	D_c, in., [cm]	L_c/D_c
35	4145 [105.3]	0.15	419 [10.6]	0.099	25.2 [64.0]	25.7 [65.3]	1.0
50	2843 [72.2]	0.2	424 [10.8]	0.068	35.0 [88.9]	20.7 [52.6]	1.7
65	2073 [52.7]	0.25	429 [10.9]	0.050	44.6 [113.3]	15.9 [40.4]	2.8
80	1704 [43.3]	0.3	433 [11.0]	0.041	53.9 [136.9]	11.3 [28.7]	4.8
95	1436 [36.5]	0.35	438 [11.1]	0.034	63.0 [160.0]	6.8 [17.3]	9.3
110	1204 [30.6]	0.4	442 [11.2]	0.029	71.5 [181.6]	2.5 [6.4]	29

ules of the SPP computer code[15] were used to calculate these values. The Reynolds number of the internal flow during the burn (based on motor diameter) equals $1-2 \times 10^7$.

A prediction of Sr_m at the cavity between the center and aft segments is provided in Table 4. It is assumed in these estimates that, as the cavity becomes wider and shallower, the momentum thickness of the shear layer within the cavity approaches that for locations just forward of the cavity and can be approximated by a linear function decreasing from $\delta = 5.5$ in. (14 cm) at $t = 40$ s to $\delta = 4$ in. (10 cm) at $t = 110$ s. U in Eq. (5) is taken as that for the center of the cavity, and f corresponds to the fundamental acoustic mode. Sr_m varies from 0.2–0.4 between $t = 50-110$ s. The maximum pressure oscillations occur when $Sr_m \sim 0.2-0.25$. This is consistent with Ref. 21, in which a hyperbolic tangent velocity profile was used, and vortex shedding was predicted for $Sr_m < 0.5$ with maximum spatial amplification for values of Sr_m around 0.2.

Evaluation of the growth rate function g is problematic because it is very sensitive to Sr_m and δ, and the predictions of these values are not exact. Vuillot et al.[22] also noted this sensitivity and recommended that the linear theory be used with caution. The function g appears to be periodic with respect to the dimensionless standoff distance, defined by L/δ. The plots in Ref. 21 also seem to indicate that g has reached a steady-state amplitude for the dimensionless standoff distances corresponding to vortex shedding around the SRMU cavity with impingement on the nozzle entrance ($L/\delta > 70$). For $Sr_m = 0.2$, 0.3, and 0.4, a half-period of the oscillatory function g equals about 8, 5, and 3, respectively. This means that negative values of g (required for a positive growth rate) exist for the SRMU in ~40-in. (102-cm) intervals at $t \sim 50$ s, in ~25-in. (64-cm) intervals at $t \sim 80$ s, and in ~10-in. (25-cm) intervals at $t \sim 110$ s. This condition is illustrated in Fig. 7, in which positive and negative regions are compared heuristically with the width of the cavity. Because of the sensitivity of the dimensionless standoff distance to the magnitude of the shear-layer momentum thickness, these regions probably do not occur as shown, but may be somewhat shifted en bloc across the cavity.

It is apparent from Fig. 7 that regions of negative g can occur around both faces of, as well as within, the cavity when $Sr_m > 0.2$. The linear theory, therefore, does not explicitly define the vortex shedding origin during most of the observed pressure oscillations. However, during the maximum pressure oscillations (with $Sr_m \sim 0.2$), the linear theory indicates that the acoustic growth rate is probably positive around only one of the faces. It will be assumed in implementation of the empirical model that vortex shedding initiates around the forward cavity face because this location is closer to the pressure node of the fundamental acoustic mode. It is interesting to note (see Table 3) that the absolute value of F is always smaller for vortex origination around the forward cavity face (and impingement of the nozzle entrance) than for origination around

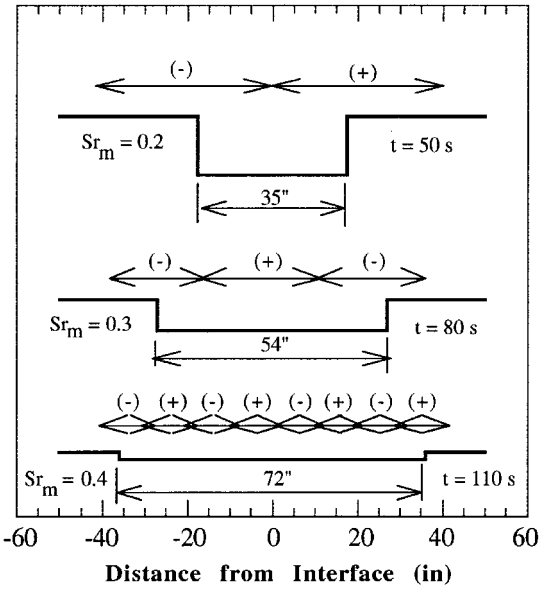

Fig. 7 Idealized cavity geometry and heuristic representation of regions of positive and negative values of growth rate function g for three time points.

the aft cavity face, which is further from the pressure node. In fact, the linear theory yields the surprising result that the largest acoustic growth rate would occur if the SRMU cavity were only one-fifth of the chamber length aft of the forward closure. This seems to contradict experimental results that show that the amplification is largest for vortex shedding near pressure nodes of the acoustic modes.[6,19]

V. Comparison of Model and Test Results

The test data are compared with the results of the empirical model in Fig. 8. The frequency tracks are in reasonable agreement with the results of Eq. (3), suggesting that vortex shedding is occurring and that an integer number of vortices fit between the center/aft segment interface and the nozzle entrance. The first frequency track corresponds to stage number $m = 5$, suggesting that vortex shedding begins with five vortices in the distance L.

This number is apparently higher than for other solid rocket motors because of the length of the SRMU aft segment. Equating the vortex shedding frequency with that of the acoustic mode of the motor (modeled as a closed-closed chamber) it can be shown that, as a rule of thumb, $m \sim$ Integer $[n/(MN)]$, in which n is the acoustic mode number, and the chamber of the motor is assumed to be divided into N segments of equal length. The number of segments column of Table 1 shows that, for comparable M values, the Titan IV SRMU stage numbers are similar to those for the Ariane 5 MPS and are higher than those for the Space Shuttle SRB or earlier Titan IV solid rocket motors.

The frequency tracks in Fig. 8 overlap in time. This is partly because vortex shedding for a particular stage number lasted longer during some tests than in others. But, as shown in Fig. 3, as many as three frequency components sometimes coexist during the burn. Since vortices are large-scale structures represented by a single instability wave, the superposition of instability waves implies that during these time points the flow inside the motor is only approximately characterized by distinct vortices between the shedding and impingement points.

The prediction for stage number $m = 6$ falls between two frequency tracks. Neither track is grossly out of agreement with the empirical model and it is possible that one or both corresponds to stage number $m = 6$ vortex shedding. The discontinuity at $t = 62$ s, however, implies that some kind of change occurred. A possible physical explanation is that the

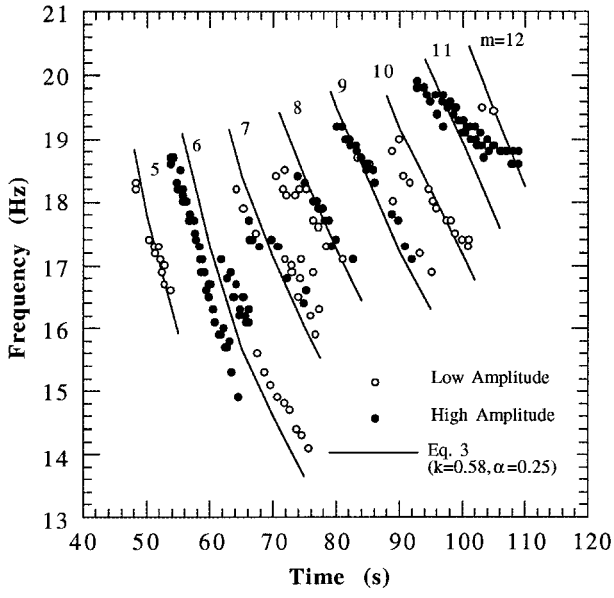

Fig. 8 Comparison of static firing test pressure oscillation frequencies with empirical relationship for vortex shedding.

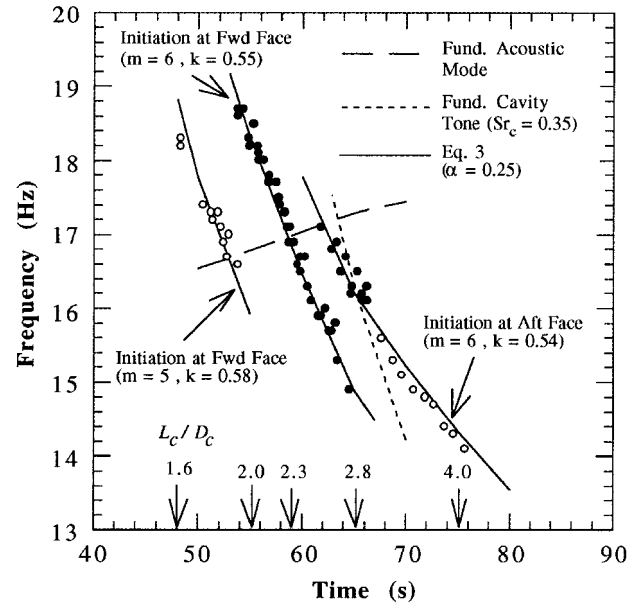

Fig. 9 Comparison of test data with postulated fundamental cavity tone, fundamental acoustic mode, and stage $m = 6$ vortex shedding.

vortex shedding point moved during this stage number to a location around the aft cavity face. Plots of Sr support this hypothesis.[8]

The value of dimensionless standoff distance L/δ for vortex origination around the forward cavity face and impingement on the aft cavity face equals about nine at $t = 62$ s. Plots in Ref. 21 suggest that g has a minimum (maximum negative value) around this standoff distance for $Sr_m = 0.2$. [The data provided in Ref. 21 correspond to a straight impingement surface perpendicular, and symmetrically placed, with respect to the plane of the shed vortices. The data also assume that the length of the impingement surface is three times the shear-layer momentum thickness. The aft cavity face for the SRMU is not planar or symmetric (see Fig. 6), but, at $t = 62$ s, has about the same length as used in Ref. 21.] The product of F (see Table 3) and g consequently predicts a positive acoustic growth rate for vortex impingement on the aft cavity face. It therefore appears possible that acoustic feedback occurred within the cavity as well as between this interface and the nozzle. In other words, a single vortex may have been entrained in the cavity, or clipped at the aft face, creating frequencies comparable to that of the fundamental acoustic mode.

The frequency variation for the postulated cavity tone $f = Sr_cU/L_c$ is shown in Fig. 9, assuming that Sr_c equals 0.35. The cavity is 43–52 in. long during the period when one vortex is apparently entrained or clipped. The average length of vortices for $m = 6$ at $t = 62$ s, however, is 71 in. This difference in length may be caused by spatial growth of the disturbance,[28] which, as mentioned earlier, results in stretching of the vortices as they travel downstream.[22] The initial vortex in this case would be shorter than the average for the vortex stream. Photographs in Ref. 31 also illustrate that a vortex does not have to fit entirely within a cavity to be destroyed.

The static firing test data, after scaling time to that for the nominal propellant burn rate, indicate that the maximum amplitudes of the pressure oscillations for all of the tests occur between $t = 59$ and 60.5 s, and that pressure pulses, with amplitudes very close to those of the maxima, occur for the PQM1′ and QM3 tests as late as 65 s (see Figs. 2b and 2c). The pressure pulses, therefore, appear to correspond to excitation of the fundamental acoustic mode by vortex impingement at both the nozzle entrance and the aft face of the cavity. A best fit of the $m = 6$ vortex shedding frequencies was obtained with a 5% reduction in the convection velocity constant, possibly caused by a change in the mean velocity profile during the maximum pressure oscillations.

The time-variant geometry of the cavity may have contributed to the initiation of the vortex shedding. Although the SRMU cavity has injecting walls and the flow within the cavity can be expected to be different from that for classical cavity tones, it is worth noting that the shear layer at the forward face for classical cavity tones is only excited for cavity length-to-depth ratios greater than about 2.[32] This ratio is indicated at the bottom of Fig. 9 for several time points. The onset of the pressure oscillations corresponds to $L_c/D_c = 1.6$.

According to the empirical model, vortex shedding around the aft cavity face does not yield frequencies that correspond to any of the other frequency tracks observed in the test data. Also, the frequency tracks for stage numbers $m = 7$–12 do not appear to be discontinuous. The vortex shedding origin, therefore, seems to occur around the forward cavity face during subsequent stages. This is consistent with Fig. 7, which shows that regions of positive acoustic growth rate exist around both cavity faces during the later time periods, and with experimental evidence that acoustic feedback is strongest for vortex origination near pressure nodes of the acoustic modes.[6,19]

VI. Limitations of Empirical Model

Strouhal numbers computed using SRMU pressure oscillation frequencies and predicted values of U and L are compared in Fig. 10 with those from the empirical model. Note that, for all of the stage numbers, the tracks for the empirical model intersect those for the static firing test data, but that the slopes are only in good agreement for stage numbers $m = 5$ and 6. The discrepancy in slope increases with respect to decreasing Mach number (increasing time) and increasing stage number.

The lack of agreement is believed to be caused by a gradual breakdown in the simple model for the acoustic feedback. Figure 11 compares the Strouhal numbers from the test data with the variation derived from the frequencies of the fundamental acoustic mode. Also included for comparison are the least-squares best-fits for the tracks. Note that as the Mach number decreases, and as the stage number increases, the slopes of the tracks approach that for the fundamental acoustic mode. For late burn times, the frequencies of the measured pressure oscillations, therefore, appear to be dominated by resonance of the motor's fundamental acoustic mode rather than by vortex

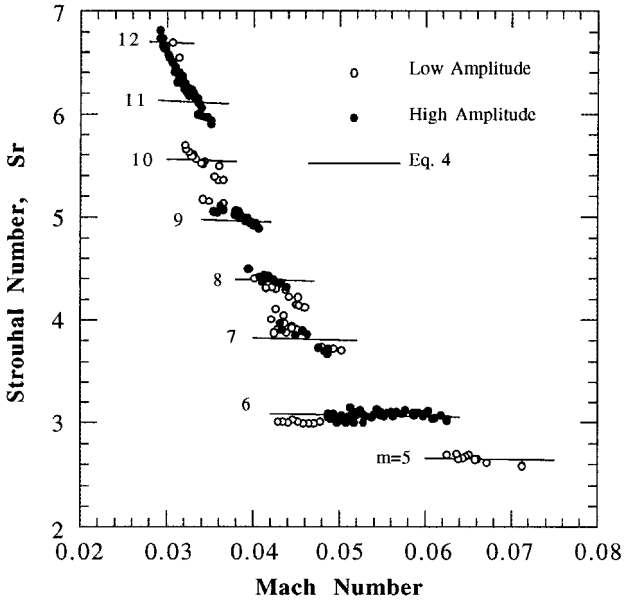

Fig. 10 Comparison of Strouhal numbers computed with static firing test data and those from the empirical relationship.

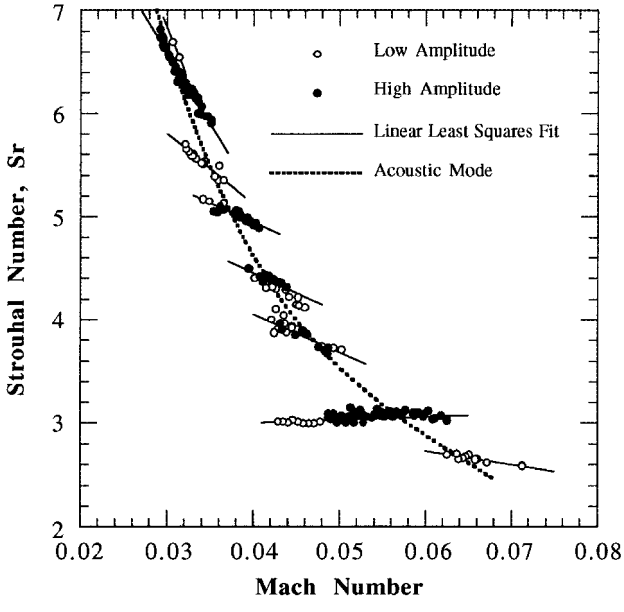

Fig. 11 Comparison of Strouhal numbers computed with static firing test data and those corresponding to resonance of the fundamental acoustic mode.

shedding as modeled by Eq. (3). In the limit the Strouhal numbers for the SRMU test data are defined by

$$Sr = f_a L/U \approx (L/2L_t)/M \tag{6}$$

in which f_a is the frequency of the acoustic mode, L_t is the distance from the forward to the aft closure, and the latter expression approximates the frequency of the fundamental acoustic mode by that for a closed-closed chamber. For the SRMU, the value in the parenthesis of Eq. (6) equals ~0.2. This trend for low Mach numbers (late burn times) is also evident in published data for the Titan 34D SRM[6] and Space Shuttle SRB,[9] and for classical cavity tones, in which it was attributed, analogously, to normal mode acoustic resonance within the cavity.[32] The Strouhal number Sr_m may be used to define a criterion for the empirical model. It is easy to show that

$$(Sr_m)_c \approx (\delta/L_t)(\pi/M_c) \tag{7}$$

where M_c is the Mach number at which resonance of the acoustic mode begins to dominate. For the SRMU, $M_c \sim 0.04$ and Eq. (7) yields $(Sr_m)_c \sim 0.3$.

VII. Conclusions

Pressure oscillations measured during static firing tests of the Titan IV SRMU are believed to be caused by coupling between the motor's fundamental acoustic mode and vortices that shed near the cavity between the center and aft segments. These vortices impinge on the SRMU nozzle and excite a shear layer that initiates around the forward cavity face, near the pressure node of the fundamental acoustic mode. The pressure oscillations appear to commence with five wavelengths in the distance between the cavity and nozzle, and this number increases to 12 before the end of burn. During the time period of the maximum pressure oscillations, a Strouhal number based on shear-layer momentum thickness is close to that predicted by linear theory for the highest acoustic growth rate. During this time period the fundamental acoustic mode may also be coupled with acoustic feedback generated by vortex impingement at both the motor nozzle and the aft face of the cavity. The vortex shedding phenomenon for the SRMU is similar to that for other large solid rocket motors, but the stage numbers and pressure oscillation amplitudes appear to be somewhat higher and lower, respectively, than for other motors. The impact of the SRMU pressure oscillations on dynamics and control of the Titan IV system is minor.

Acknowledgments

This work was supported by the U.S. Air Force Material Command, Space and Missile Systems Center under Contract F04701-93-C-0094. The authors wish to thank J. W. Murdock and G. R. Spedding for many helpful discussions. The authors are also grateful to I.-S. Chang for recovering the CFD data for implementation of the linear theory.

References

[1]Hercules Aerospace Company, Missiles, Ordnance, & Space Group, Bacchus Works, "Titan IV QM-4 Solid Rocket Motor Upgrade (SRMU) Full Scale Static Final Report," Contract F04701-85-C-0019, Subcontract KH7-163000, Data Item Description SR-T05-008-3, Magna, UT, Oct. 1993.

[2]Hercules Aerospace Company, Missiles, Ordnance, & Space Group, Bacchus Works, "Specific Test Plan for Titan IV Static Firing of PQM-1 (Prime)," Contract KH7-163000, DRD SR-T05-003, Magna, UT, Dec. 1991.

[3]Bruce, J. R., "Internal SRMU Pressure Oscillation at 18 Hz: Action Item 1.1," Loads Technical Working Group Meeting, Martin Marietta Technologies, Inc., April 1994.

[4]Culick, F. E. C., "Combustion Instability in Solid Rocket Motors, Vol. II: A Guide For Motor Designers," Prepared by JANNAF Combustion Subcommittee, Chemical Propulsion Information Agency, Johns Hopkins Univ., Applied Physics Lab., Laurel, MD, Jan. 1981.

[5]Isakowitz, S. J., *International Reference Guide to Space Launch Systems*, 2nd ed., AIAA, Washington, DC, 1991.

[6]Brown, R. S., Dunlap, R., Young, S. W., and Waugh, R. C., "Vortex Shedding as a Source of Acoustic Energy in Segmented Solid Rockets," *Journal of Spacecraft*, Vol. 18, No. 4, 1981, pp. 312–319.

[7]Brown, R. S., "Combustion Instability in Solid Propellant Motors," *Proceedings of the AIAA/SAE/ASME/ASEE Solid Rocket Motor Combustion Instability Workshop, 31st Joint Propulsion Conference* (San Diego, CA), AIAA Solid Rocket Technical Committee, AIAA, Washington, DC, 1995, pp. 17–26.

[8]Dotson, K. W., Koshigoe, S., and Pace, K. K., "Vortex Driven Pressure Oscillations in the Titan IV Solid Rocket Motor Upgrade," AIAA Paper 95-2732, July 1995.

[9]Nesman, T., "RSRM—Chamber Pressure Oscillations: Full Scale Ground and Flight Test Summary and Air Flow Test Results," *Proceedings of the AIAA/SAE/ASME/ASEE Solid Rocket Motor Combustion Instability Workshop, 31st Joint Propulsion Conference* (San Diego, CA), AIAA Solid Rocket Technical Committee, AIAA, Washington, DC, 1995, pp. 27–48.

[10]Scippa, S., Pascal, P., and Zanier, F., "Ariane 5—MPS—Chamber Pressure Oscillations Full Scale Firings Results Analysis and Further Studies," AIAA Paper 94-3068, June 1994.

[11]Leuridan, J., Van Der Auweraer, H., and Vold, H., "The Analysis of Nonstationary Dynamic Signals," *Journal of Sound and Vibration*, Vol. 28, No. 8, 1994, pp. 14–26.

[12]Papoulis, A., *Signal Analysis*, McGraw–Hill, New York, 1977, pp. 162–164, 248–251.

[13]Duron, Z. H., "Spectral Analysis of Pressure Fluctuations in SRM Firings," *Proceedings of the AIAA/SAE/ASME/ASEE Solid Rocket Motor Combustion Instability Workshop, 31st Joint Propulsion Conference* (San Diego, CA), AIAA Solid Rocket Technical Committee, AIAA, Washington, DC, 1995, pp. 49–57.

[14]Vold, H., and Crowley, J., "Time Variant Spectral Analysis Applications Using the Maximum Entropy Method," *Proceedings of the 6th International Modal Analysis Conference* (Orlando, FL), Union College, Schenectady, NY, 1988, pp. 1403–1406.

[15]Nickerson, G. R., Culick, F. E. C., and Dang, A. L., "Solid Propellant Rocket Motor Performance Computer Program (SPP), Version 6.0," Air Force Astronautics Lab., TR-87-078, Dec. 1987.

[16]Flatau, A., and VanMoorhem, W., "Prediction of Vortex Shedding Responses in Segmented Solid Rocket Motors," AIAA Paper 90-2073, July 1990.

[17]Flandro, G. A., and Jacobs, H. R., "Vortex-Generated Sound in Cavities," AIAA Paper 73-1014, Oct. 1973.

[18]Culick, F. E. C., and Magiawala, K., "Excitation of Acoustic Modes in a Chamber by Vortex Shedding," *Journal of Sound and Vibration*, Vol. 64, No. 3, 1979, pp. 455–457.

[19]Dunlap, R., and Brown, R. S., "Exploratory Experiments on Acoustic Oscillations Driven by Periodic Vortex Shedding," *AIAA Journal*, Vol. 19, No. 3, 1981, pp. 408, 409.

[20]Nomoto, H., and Culick, F. E. C., "An Experimental Investigation of Pure Tone Generation by Vortex Shedding in a Duct," *Journal of Sound and Vibration*, Vol. 84, No. 2, 1982, pp. 247–252.

[21]Flandro, G. A., "Vortex Driving Mechanism in Oscillatory Rocket Flows," *Journal of Propulsion and Power*, Vol. 2, No. 3, 1986, pp. 206–214.

[22]Vuillot, F., Traineau, J. C., Prevost, M., and Lupoglazoff, N., "Experimental Validation of Stability Assessment Methods for Segmented Solid Propellant Motors," AIAA Paper 93-1883, June 1993.

[23]Vuillot, F., Lupoglazoff, N., Prevost, M., and Traineau, J. C., "Improved Modelisation for Numerical Simulation of Oscillatory Solid Rocket Motors," *Proceedings of the AIAA/SAE/ASME/ASEE Solid Rocket Motor Combustion Instability Workshop, 31st Joint Propulsion Conference* (San Diego, CA), AIAA Solid Rocket Technical Committee, AIAA, Washington, DC, 1995, pp. 58–79.

[24]Kourta, A., "Vortex Shedding in Segmented Solid Rocket Motors," *Journal of Propulsion and Power*, Vol. 12, No. 2, 1996, pp. 371–376.

[25]Rockwell, D., "Oscillations of Impinging Shear Layers," *AIAA Journal*, Vol. 21, No. 5, 1983, pp. 645–664.

[26]Rossiter, J. E., "Wind-Tunnel Experiments on the Flow over Rectangular Cavities at Subsonic and Transonic Speeds," Aeronautical Research Council, Ministry of Aviation, Reports and Memoranda 3438, London, Oct. 1964.

[27]Jou, W.-H., and Menon, S., "Modes of Oscillation in a Nonreacting Ramjet Combustor Flow," *Journal of Propulsion and Power*, Vol. 6, No. 5, 1990, pp. 535–543.

[28]Michalke, A., "The Instability of Free Shear Layers: A Survey on the State of the Art," *Progress in Aerospace Sciences*, Vol. 12, Pergamon, New York, 1972, pp. 213–239.

[29]Heller, H. H., and Bliss, D. B., "Aerodynamically Induced Pressure Oscillations in Cavities—Physical Mechanisms and Suppression Concepts," Defense Technical Information Center, Air Force Flight Dynamics Lab., TR-74-133, Wright–Patterson AFB, OH, Feb. 1975.

[30]Chang, I.-S., Patel, N. R., and Yang, S., "Titan IV Motor Failure and Redesign Analyses," *Journal of Spacecraft and Rockets*, Vol. 32, No. 4, 1995, pp. 612–618.

[31]Rockwell, D., and Naudascher, E., "Self-Sustained Oscillations of Impinging Free Shear Layers," *Annual Review of Fluid Mechanics*, Vol. 11, 1979, pp. 67–94.

[32]Tam, C. K. W., and Block, P. J. W., "On the Tones and Pressure Oscillations Induced by Flow over Rectangular Cavities," *Journal of Fluid Mechanics*, Vol. 89, Pt. 2, 1978, pp. 373–399.